Soft Matter

# Impact of Surface Hydrophilicity on the Ordering and Transport Properties of Bicontinuous Microemulsions



| | |
|---|---|
| Journal: | *Soft Matter* |
| Manuscript ID | SM-ART-06-2024-000728.R1 |
| Article Type: | Paper |
| Date Submitted by the Author: | 06-Sep-2024 |





| | |
|---|---|
| Complete List of Authors: | Heroux, Luke; Oak Ridge National Laboratory<br>Ojedeji, Damilola; University of Tennessee Knoxville, Chemical and Biomolecular Engineering<br>Barth, Brian; University of Tennessee Knoxville, Chemical and Biomolecular Engineering<br>Imel, Adam; University of Tennessee Knoxville, UT-ORII<br>Doxastakis, Manolis; University of Tennessee, Chemical and Biomolecular Engineering<br>Zawodzinski, Thomas; The University of Tennessee Knoxville; Oak Ridge National Laboratory<br>Dadmun, Mark; The University of Tennessee Knoxville, Chemistry |
| | |

# Impact of Surface Hydrophilicity on the Ordering and Transport Properties of Bicontinuous Microemulsions

Luke Heroux (orcid.org/0000-0001-8993-3904)[1,2], Damilola Ojedeji (orcid.org/0009-0007-3923-2721)[3], Brian Barth (orcid.org/0000-0002-3887-6054)[3], Adam Imel (orcid.org/0000-0002-3177-7846)[4], Manolis Doxastakis* (orcid.org/0000-0002-9175-9906)[3], Tom Zawodzinski (orcid.org/0000-0002-2690-8784)[3,5], Mark Dadmun* (orcid.org/0000-0003-4304-6087)[6]

1-University of Tennessee, Department of Material Science and Engineering

2-Oak Ridge National Laboratory, Neutron Scattering Division

3-University of Tennessee, Department of Chemical and Biomolecular Engineering

4-University of Tennessee – Oak Ridge Innovation Institute

5- Oak Ridge National Laboratory, Chemical Sciences Division

6-University of Tennessee, Department of Chemistry

*Corresponding authors (edoxasta@utk.edu and dad@utk.edu)

## Abstract

Microemulsions (MEs) have many industrial applications, where recent developments have shown that MEs can be utilized for electrochemical applications, including potentially in redox flow batteries. However, understanding the structure and dynamics of these systems, including at a surface, is needed to direct and rationally control their electrochemical behavior. While bulk solution measurements have provided insight into

their structure, their assembly at an interface also impacts the electron (to the electrode) and ion (across the surfactant) charge transfer processes in the system. To address this shortcoming, neutron reflectivity experiments and molecular simulations have been completed that document the near surface structure of a series of deuterated water ($D_2O$)/Polysorbate-20/Toluene MEs on hydrophilic and amphiphilic surfaces. These results show that the microemulsions form complex layered structures near a hard electrode surface, where most layers are not purely one component. Decreasing the $D_2O$ concentration in the ME increases the number of and purity of the layers established on the solid surface. These lamellar-type layers transition from the surface to the bulk microemulsion as a series of mixed layers (i.e., containing oil, water, and surfactant) that are consistent with perforated lamellae. Additionally, these mixed lamellae appear to become more perforated with oil and water pathways on an amphiphilic surface. The purity and thickness of these layers will influence the accessibility of an electrode by redox active species, as well as ion transport required to satisfy the electroneutrality condition.

## Introduction

Interest in microemulsions (MEs) has spanned several decades, where research efforts focused on their use in various industrial applications from food products to pharmaceuticals and healthcare to energy materials, with a recent concentration on their electrochemical functionality for use in energy-related devices.[1,2,3,4,5] MEs consist of oil, water, and surfactants that consist of a hydrophilic head group and a hydrophobic tail group.[6,7] The head and tail of the surfactant molecules arrange at the interface between the immiscible oil and water, where the hydrophilic head aligns with the water phase, while the hydrophobic tail aligns with the oil/non-polar phase. These mixtures generally create one of 3 general types of microemulsions, oil droplets in water (O/W), water droplets in oil (W/O), or a bicontinuous microemulsion (BME).[6-10] BMEs, also known as Winsor III type-microemulsions, are low viscosity, isotropic, structured mixtures that naturally occur when separate continuous oil and water channels form with the surfactant acting as the boundary between the two, lowering the interfacial tension between the oil channel and the water channel.[7,9,10] Research has shown that BME structures consist of well-distributed channels in the bulk.[5,10] However, preferential layering of the oil and water at solid surfaces occurs due to the polarities of the surface, oil, water, and surfactant, leading to an interruption of the bicontinuous morphology in a region near the surface, impacting transport properties.[11-14] This ordering at the surface is important given that, until more recently, research on the electrochemical behavior of microemulsions has focused on the bulk structure of these systems, with few studies focusing on the impact of surface morphology on their performance.[4,12-17] Measurements of the assembly of BMEs in variable environments, such as temperature or electric field, have shown that the structure of the

microemulsion can vary significantly with a change of conditions.[17,18,19] The electrochemistry of BMEs in the bulk has been previously examined to demonstrate this evolution of the BME structure.[17,18]

In electrochemical applications, electron transport must occur at or near the electrode surface, where the electrode hydrophobicity can vary with the polarity of the electrode material. This variation in polarity, ranging from hydrophilic to hydrophobic, can direct the ME structure at the surface, which can differ substantially from that of the bulk structure.[11,13,20,21,22] To understand how the surface ordering of a ME relates to electrochemical performance, the self-assembly of the ME near an impenetrable surface must be determined over a variety of hydrophilicities to provide insight into the behavior of the ME near a range of potential electrode surfaces. Neutron reflectivity is one method that provides the required resolution and contrast control to determine the surface ordering of MEs for this purpose.[21,23] Using deuterated water ($D_2O$) in the microemulsion system, the contrast in scattering length density (SLD) between the protonated oil/surfactant and the $D_2O$ increases. This strong contrast provides the required resolution to elucidate the structure of the surfactant/oil and water mixture in the system and is used to determine the morphology of the microemulsion at a surface.[14] Previous studies have shown that bicontinuous microemulsions may form lamellar-like, ordered structures at a hard surface that can vary with surface polarity.[13,20,23,24] These lamellae may also perforate as more well-ordered near-surface layers transition to the bicontinuous structure of the bulk. The layered structure and transition to a bicontinuous bulk are dependent on the surface polarity and the presence of an applied stress parallel to the interface.[15,23] Growing interest in renewable energy devices has increased research on microemulsions for

electrochemical storage devices, focusing on the lamellar structures that form at the surface of the electrode and how the functionality of the device changes with these structures.[2,4,9,20]

Recent studies have shown that the phase structure of microemulsions does not inhibit the transfer of electrons at the surface of an electrode or the transfer of ions within the microemulsion between the oil and water phases.[4,25] Bard, *et al*. demonstrated electron and ion transfer using cyclic voltammetry and collision experiments, where the addition of an ionic liquid allowed both electron transfer and ion transfer.[25] It is postulated that when the electron transfers from a redox active agent, either a negative ion transfers out of or a positive ion may transfer into the aqueous phase through the surfactant. Peng *et al*. also observed that structuring in a 66% water BME at the surface allowed the transfer of electrons from the electrode to the ferrocenium ion with a compensatory transfer of an ion across the non-polar layer into the aqueous solution.[4]

Previous small angle neutron scattering studies by our group have carefully determined the phase behavior of polysorbate-20/toluene/water microemulsions over a broad composition range,[17] where this microemulsion is that which is examined by Peng[4] and is examined in this manuscript. These SANS results show that this microemulsion forms a bicontinuous phase over a broad composition range, ca. 20-80% water. The bicontinuous channels in the microemulsion examined in this study are 48 Å on average and form layers on an amphiphilic electrode.[4,17] To understand the correlation of the ordering of this microemulsion near a surface to its electrochemical performance, we have explored the near surface ordering of a series of bicontinuous microemulsions on surfaces of varying

hydrophilicity. Neutron reflectivity monitors the surface structure of BMEs as a function of microemulsion composition, where the microemulsion incorporates deuterated water to increase contrast in the scattering experiments. The ordering of the bicontinuous microemulsion near the impenetrable surfaces provides insight into the role of surface ordering on the electrochemical performance of BMEs. These surface measurements can also provide guidance to design electrode surfaces for improved performance in electrochemical applications.

## Experimental methods

### *Microemulsion Preparation*

All ME compositions were prepared by using an 82.5% polysorbate-20 (poly(ethylene glycol) (20) sorbitan monolaurate, Sigma Aldrich, St Louis, MO), 17.5% 1-butanol (purity >99%, Sigma Aldrich), by mass as the emulsifier. The emulsifier then had a constant 10:1 mass ratio with the oil. In these mixtures, the polysorbate-20 serves as the surfactant, and the 1-butanol is the co-surfactant helping reduce the interfacial tension further. For neutron reflectivity, MEs were prepared as 80% $D_2O$, 60% $D_2O$, and 30% $D_2O$, by volume. The remaining contents of the microemulsion were an emulsifier/toluene (high-performance liquid chromatography [HPLC] grade, Fisher Scientific, Pittsburgh, PA) mixture. ME compositions studied are presented in the ternary phase diagram of the Polysorbate-20/Toluene/$D_2O$ system in Figure 1. Additionally, the phase diagram shows the phase boundary between the two-phase and one-phase regions, as previously reported for this system, showing that all compositions are in the one-phase region.[4]

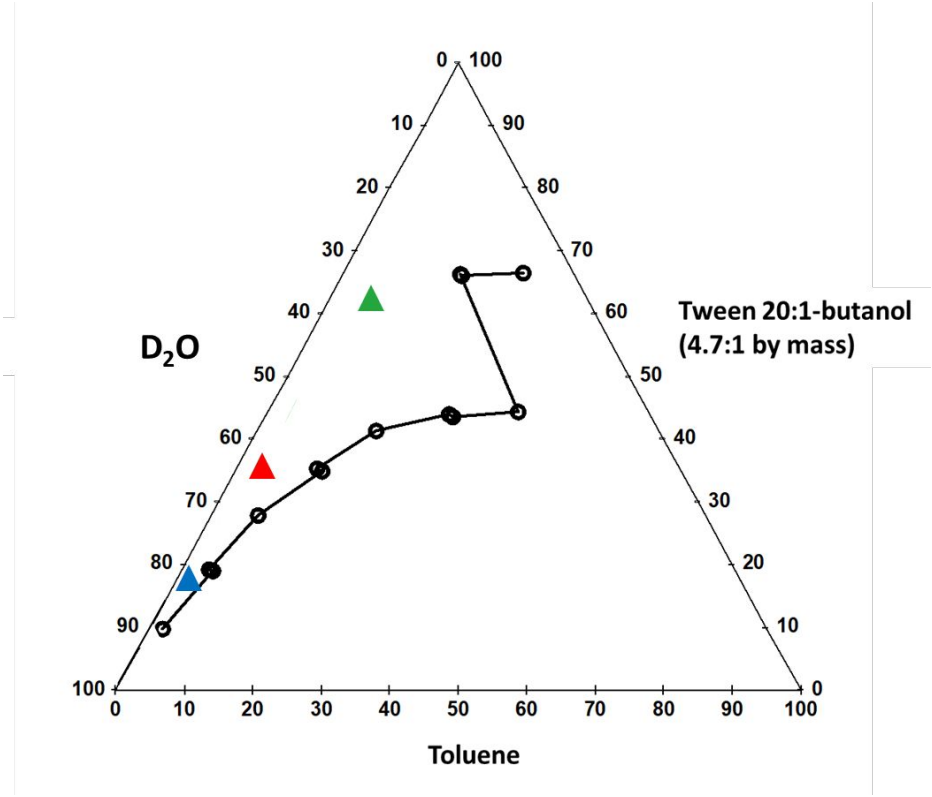


Figure 1 – Ternary phase diagram of microemulsion examined, including concentrations studied in neutron reflectivity measurements. Colored triangles indicate examined compositions (30% $D_2O$- green, 60% $D_2O$-red, and 80% $D_2O$-blue). Black line indicates phase boundary between 1 and 2 phase domains.

*Neutron Reflectometry*

Silicon substrates of varying hydrophilicity were prepared in advance of the neutron scattering experiments. Each silicon wafer was first cleaned with a piranha solution (3:1 sulfuric acid/hydrogen peroxide) to remove any surface contaminants. Both Si wafers were then exposed to UV-Ozone to create a controlled hydrophilic silicon oxide surface.

The first Si wafer, referred to as the hydrophilic substrate, was then used as prepared. The other Si wafer was transferred to a glove box, where an amphiphilic surface was prepared by silanization of the wafer. The reaction proceeded by placing the oxidized wafer in a 4 wt% n-octadecyltrimethoxysilane solution in toluene for three days. The amphiphilic

substrate was then sonicated in toluene for 30 minutes prior to being rinsed with toluene and dried with air. The water contact angle of each substrate was then determined to quantify its hydrophilicity, where the hydrophilic substrate was found to have a water contact angle of 23°, while the amphiphilic substrate has a water contact angle of 66°, that replicates that of a glassy carbon electrode surface.[22] This is considered an amphiphilic surface because the static water contact angle is greater than that of the hydrophilic surface but does not have a water contact angle greater than 90°.

Neutron reflectivity measurements were performed at ambient temperature (T≈25°C) on the NG7 horizontal axis reflectometer at the NIST Center for Neutron Research. The MEs were loaded into a solution cell on the horizontal axis reflectometer, where the neutrons travel through the Si substrate to the $SiO_x$-microemulsion interface. Neutrons then reflect off the structure at the interface, where changing the incident angle controls the depth of the scattered neutrons.[26,27] The resulting intensity of reflected neutrons is then recorded as a function of wavevector, Q, which is defined as, $Q = \frac{4\pi \sin(2\theta)}{\lambda}$. In this equation, λ is the wavelength of the neutrons, and 2θ is the angle of reflection. ME samples were loaded as prepared into solution cells with either the hydrophilic (Silicon oxide) substrate or the amphiphilic (Silane) substrate. Reflectivity curves were obtained over a Q-range of 0.005 $Å^{-1}$ to 0.15 $Å^{-1}$. Data reduction was performed using Reductus software, and data analysis was performed by fitting the measured reflectivity curve to a multi-layer model using IGOR Pro 8 with the Motofit add-on for reflectometry.[28,29] Fits were performed using least-squares methods to minimize the error between the measured data and the calculated fit, where the quality of the fit is reported as the square of the gradient $\chi^2$. Initially, genetic

optimization was applied to find global minimum $\chi^2$, followed by the Levenberg-Marquardt method to find the local minimum $\chi^2$.[27] $\chi^2$ is calculated using Equation 1, where L is the number of points in the data, $y_{n,obs}$ represents the observed intensity of the reflected neutron beam, while $y_{n,calc}$ is the calculated intensity in the least-squares fit, and $y_{n,err}$ is the local error between the fitted value and the actual measurements.[29]

$$\chi^2 = \sum_{n=1}^{L} \frac{1}{L}\left(\frac{y_{n,\,obs} - y_{n,\,calc}}{y_{n,\,err}}\right)^2 \qquad \text{Equation 1}$$

$$\rho_z = \sum_{i=0}^{N} \frac{\rho_i - \rho_{i+1}}{2}\left(1 + erf\,\frac{z - z_i}{\sqrt{2\sigma_i}}\right) \qquad \text{Equation 2}$$

The SLD profile, $\rho_z$, is then determined using Equation 2, where N is the total number of layers, ρ is the scattering length density of each layer, *erf* is the error function, *z* is the distance from the solid-liquid interface, and σ is the roughness between the layers. This fitting procedure is valid if σ is small compared to the neighboring layer thicknesses, which is true for all of the fits provided below. To put additional constraints on the fitting of the reflectivity data, the mass balance of the $D_2O$ in the model scattering length density profile of each microemulsion were calculated and fits where this value deviated more than 10% from the composition of the sample were discarded. The mass balance, MB, in each microemulsion across the surface structure was calculated using Equation 3,

$$MB = \int Vol.Frac.of D_2O(z)dz = \int \frac{SLD_{D2O-} - SLD_{meas}(z)}{SLD_{D2O-} - SLD_{oil+surf}}\,dz, \qquad \text{Equation 3}$$

In Equation 3, $SLD_{D_2O}$ is the scattering length density of the $D_2O$ (ca. 6.393x10$^{-6}$ Å$^{-2}$), $SLD_{meas}(z)$ is the scattering length density of the microemulsion at depth $z$, and $SLD_{oil+surf}$ is the total scattering length density of the protonated components of toluene and the surfactant (ca. 4.83x10$^{-7}$ Å$^{-2}$). The composition profiles of the layers were calculated as a function of distance from the solid-liquid interface. The mass balance results, shown in Table 1, in all reported models were within ±5% of the sample composition.

Table 1- Calculated mass balances of $D_2O$ in model fits as calculated from Equation 3.

| Substrate | 30% $D_2O$ | 60% $D_2O$ | 80% $D_2O$ |
|---|---|---|---|
| Hydrophilic Si | 32.69±0.03% | 61.94±1.70% | 75.27±0.70% |
| Amphiphilic Silane | 29.97±1.55% | 60.85±1.15% | 80.10±0.03% |

*Electrochemistry*

Electrochemical experiments were performed using a Bio-Logic VMP-3 potentiostat operated with EC-Lab V11.31 (BioLogic) software at ambient temperature (T≈25°C). Glassy carbon (3mm diameter), Pt (3mm diameter), and Au (1.6mm diameter) working electrodes were used in conjunction with a saturated calomel electrode (SCE) reference electrode and a Pt wire counter electrode purchased from BASi (U.S.). Cyclic voltammetry was performed using a 10mV/s scan rate and the resulting voltammograms were iR-compensated based on the solution resistance obtained from potentiostatic impedance spectroscopy.

*Computational Studies*

Models

The molecules in our model microemulsion (toluene, polysorbate-20, butanol, and water), as well as surfaces with varying polarities, were described by the coarse-grained (CG) MARTINI 3.0 forcefield.[30] Earlier versions of the MARTINI forcefield have been successfully employed to model these compounds.[31,32] Nonetheless, Martini 3 offers a larger parameter set, providing increased flexibility in tuning interactions between groups of atoms lumped into single particles to best reproduce bulk ME data. Figure 2 presents the mapping employed for different molecules: three bonded beads formed a single toluene molecule, two beads for butanol, while a single particle corresponds to four water molecules. All parameters utilized for toluene, butanol, and water were introduced following the study by Souza and co-workers.[30]

Modeling Polysorbate-20 formulations poses additional challenges due to the diverse composition of commercially provided Polysorbate-20, which typically includes a mixture of several distinct chemical compounds. Various polysorbates, polyisosorbates, and polysorbitols with different distributions of polyethylene glycol chain lengths, numbers, and lengths of oleate tails, as well as various stereoisomers and constitutional isomers can be found in the surfactant formulations.[33,34,35] Our focus herein was to represent the phase diagram of the Polysorbate-20/butanol/water/toluene system accurately. The Polysorbate-20 composition used in the experiments in this study comprised 40% myristic, palmitic, and stearic acids, and 60% lauric acid. Consequently, Polysorbate-20 was modeled with 60% of the molecules featuring a lauric acid tail (C12) while the remaining 40% was approximated as palmitic acid (C16).

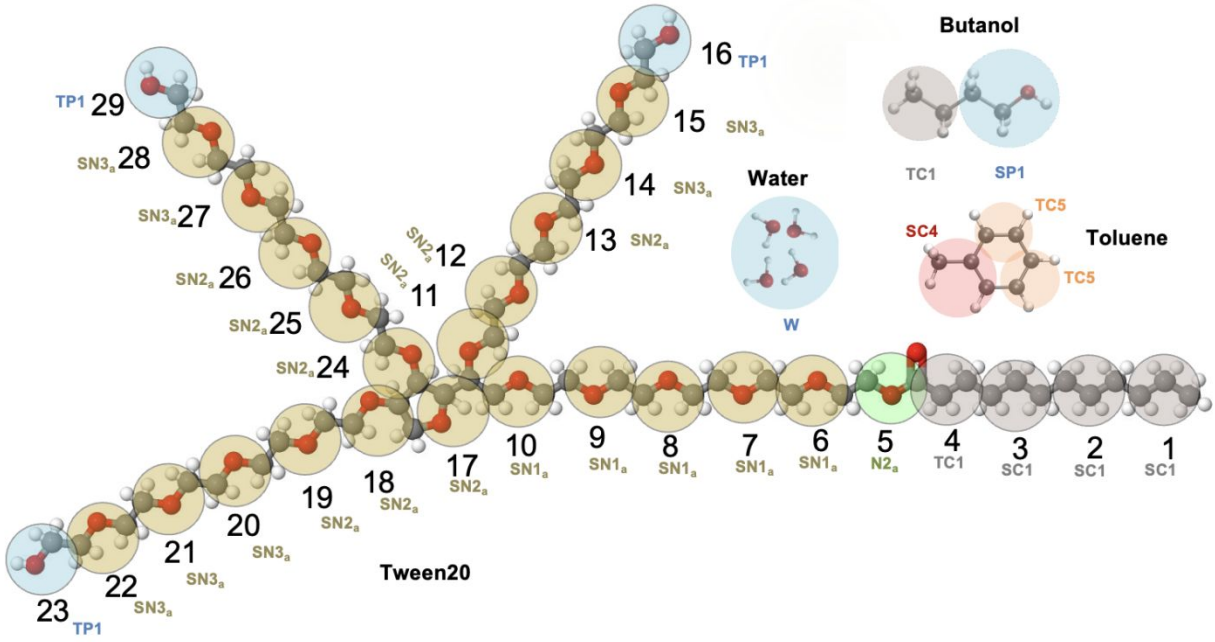


Figure 2: Coarse-grained representations of polysorbate 20 molecule with lauric acid tail (C12), butanol, toluene, and water.

The coarse grained Polysorbate-20 structure was adopted from studies by Katiyar and Singh[32] for Polysorbate-20 and Amani *et al.*[36] for polysorbate-80. Given the increased flexibility with bead size selection in MARTINI 3.0, beads with two heavy atoms like -C-O-H- were simulated as "tiny" beads. Those comprising three heavy atoms, such as -C-O-C- and -C-C-C- groups were modeled as a single "small" bead. Beads containing four heavy atoms, like -C-O-C=O- and -C-C-C-C- groups (as in the case of the palmitic acid tail model), were represented as one "regular" bead.[30] Bonded parameters were taken from Rossi *et al.*'s[37] suggestions for polyethylene glycol. Non-bonded parameters for the alkyl tail were depicted using the SC1 (C1 in the case of the palmitic acid model) bead type, commonly used for alkane molecules.[32,37,38] The alcohol end groups of the Polysorbate-20 heads (C-OH) and the -C-O-C-

O- groups were modeled using TP1 and N2a, respectively, as proposed by Souza *et al.*[30] In our study, the ethylene oxide (-C-O-C-) groups were the only units fine-tuned to capture the phase diagram, with assignments of polarity ranging between SN1a and SN3a, consistent with the range used in past ethylene oxide modeling. [31,32,36,37,38]

The surfaces were constructed based on an amorphous silica slab template, utilizing the atomistic model obtained from Pandey *et al.*.[39] An atomistic silica slab model of dimensions 884 X 936 Å was selected as a template for coarse graining. O-Si-O and O-Si-O-H groups were represented as regular beads for the interior and surface of the amorphous material, respectively, with beads positioned at the center of the silica atoms of the atomistic model, as illustrated in Figure 3. Hydrogen atoms were bonded to the unsaturated oxygen atoms, forming silanol (Si-OH) groups, and were identified separately as surface groups. The bonding of the CG beads was aligned to match the distribution of separations between Si atoms that share covalently bonded O atoms in the atomistic model. The bonds between CG beads had an equilibrium distance of 3.035 Å and harmonic force constants of 255 kJ/(mol Å$^2$). The coarse grained 884X936 silica slab shown in Figure 3 was laterally replicated three times to achieve the appropriate dimension for this study, ensuring correct bonding between edge beads in the enlarged model.

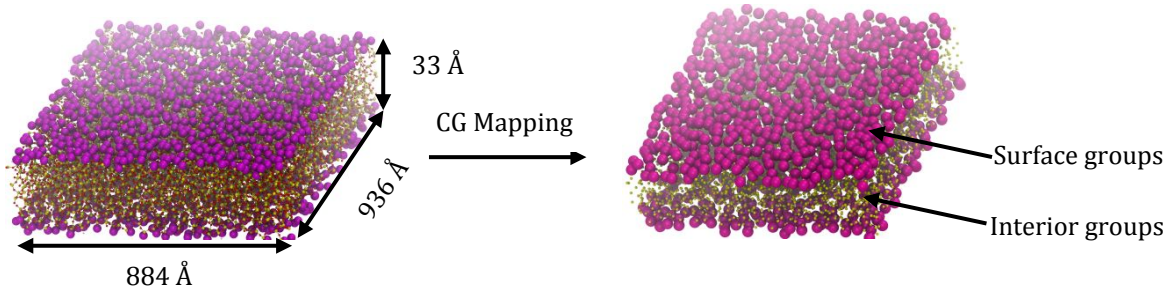


Figure 3: Atomistic and coarse-grained models of amorphous silica with surface and interior groups labeled separately.

The interior groups (Si3) were represented as SC1 for both hydrophilic and amphiphilic surfaces. Adjusting the non-bonded parameters of the surface groups (O-Si-OH) (ranging from SC2 to SN6) provided a facile route towards varying polarity of the model surface and matching the water contact angle of the systems used in the NR experiments.

Methods

Simulations were performed with the open-source software GROMACS 2023.3.[40] Coarse-grained simulations were carried out in the NPT ensemble with a semi-isotropic pressure coupling. The pressure and temperature were maintained at 1 atm and 298K, respectively, utilizing the C-rescale[41] and v-rescale algorithms,[41] with relaxation times set to 1.0 and 0.1ps for the barostat and thermostat. A cutoff of 1.1 nm was implemented for all non-bonded interactions, and a time step of 20 fs was utilized, following the recommendation of Souza et al.[30]

Phase behavior of model CG systems

To fine-tune the Polysorbate-20 model, we assessed its ability to replicate the phase diagram of the polysorbate-20/1-butanol/water/toluene system as reported in Peng *et al.*[4] Figure 4 illustrates the key features of the phase diagram of Polysorbate-20/1-butanol/water/toluene, showing both the microemulsion and two-phase regions.

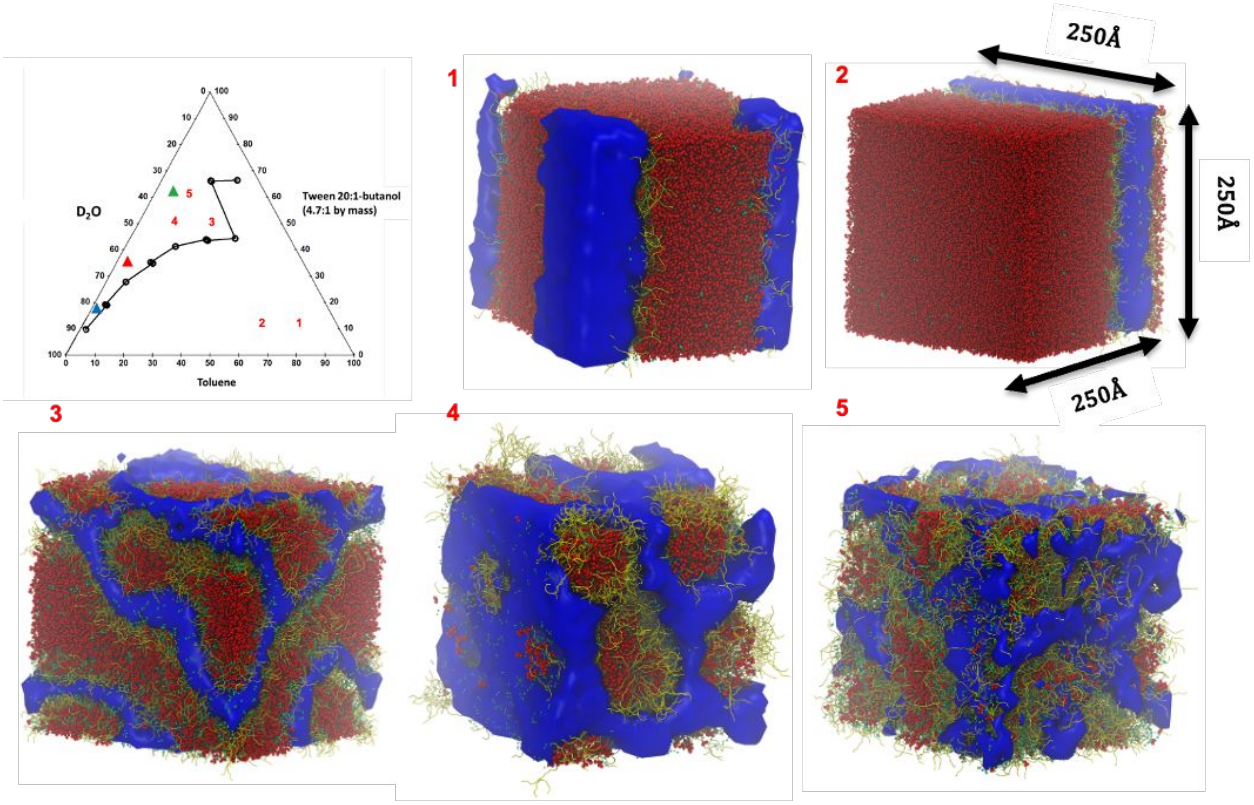


Figure 4: Reproducing the phase diagram of Toluene/water/polysorbate-20/butanol (top left) for compositions 1 (75% toluene, 12.5% water, and 12.5% polysorbate-20+butanol), 2 (62.5% toluene, 25% water, and 12.5% polysorbate-20+butanol), 3 (25% toluene, 25% water 50%, and polysorbate-20+butanol), 4 (12.5% toluene, 37.5% water, and 50% polysorbate-20+butanol) and 5 (12.5% toluene, 25% water, and 62.5% polysorbate-20+butanol) Blue: water, red: toluene, yellow: polysorbate-20, green: butanol.

Selected compositions from the phase diagram were modeled to test that the forcefield accurately reproduces the expected phases. As depicted in Figure 4, compositions 1 and 2 represent two phase regions, while compositions 3, 4 and 5 correspond to a single-phase region (bicontinuous). Our model accurately captures the phases of these compositions, initially identified by visualizing sampled configurations using VMD.[42] Beyond visual inspection, we characterized further the bicontinuous phase in our simulation through

cluster analysis, which is in line with the approach outlined by Lopian *et al.*,[43] thereby confirming the 3D connectivity of water and oil domains in the system.

## Results and Discussion

### *Reflectivity Results*

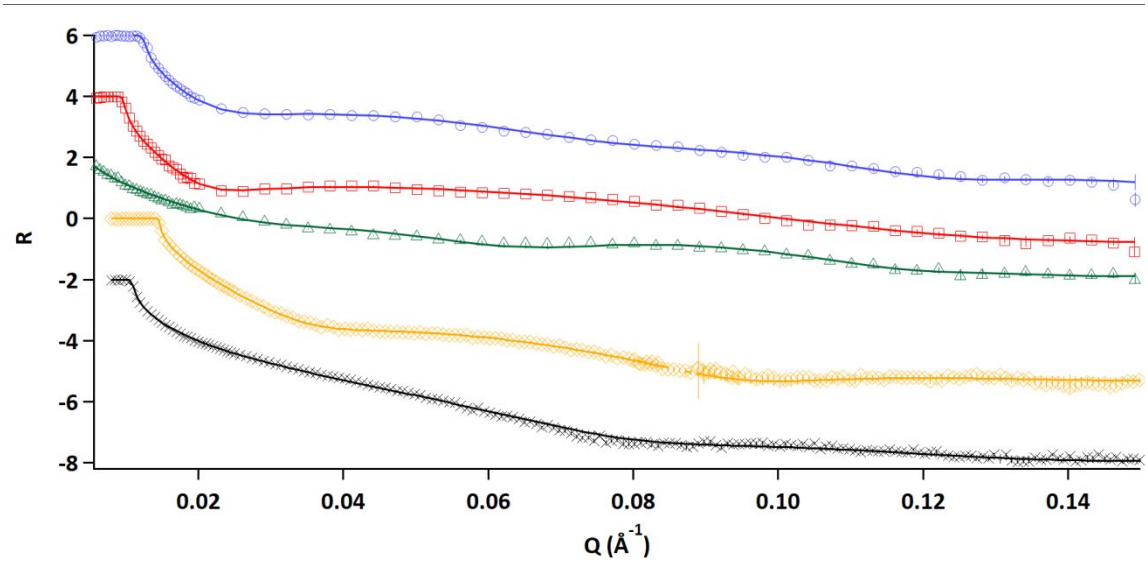


Figure 5 – Neutron reflectivity data and fits of Dry (black), Wet (orange), 30% $D_2O$ (green), 60% $D_2O$ (red), and 80% $D_2O$ (blue) on hydrophilic Si Substrate.

Neutron reflectivity data for the hydrophilic wafer that is dry, in contact with $D_2O$, and in contact with all three MEs are presented in Figure 5. In contrast, Figure 6 shows the reflectivity curves for these same conditions for the amphiphilic wafer. Figures 5 and 6 also include the fits to the experimental data using the multi-layer model to determine the structure of each ME near the hydrophilic and amphiphilic surfaces.

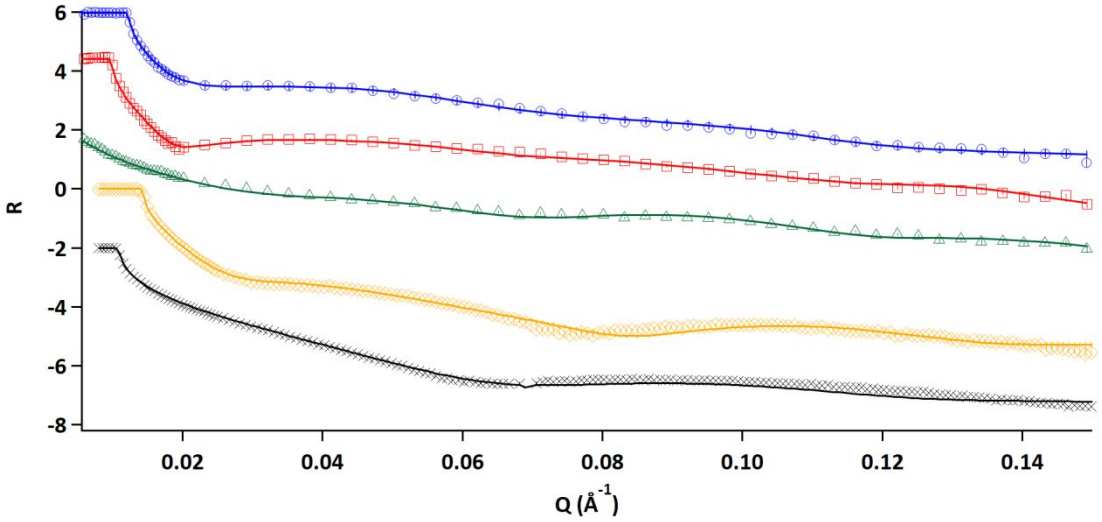


Figure 6 – Neutron Reflectometry data and fits of Dry (black), Wet (orange), 30% $D_2O$ (green), 60% $D_2O$ (red), and 80% $D_2O$ (blue) on amphiphilic Si Substrate.

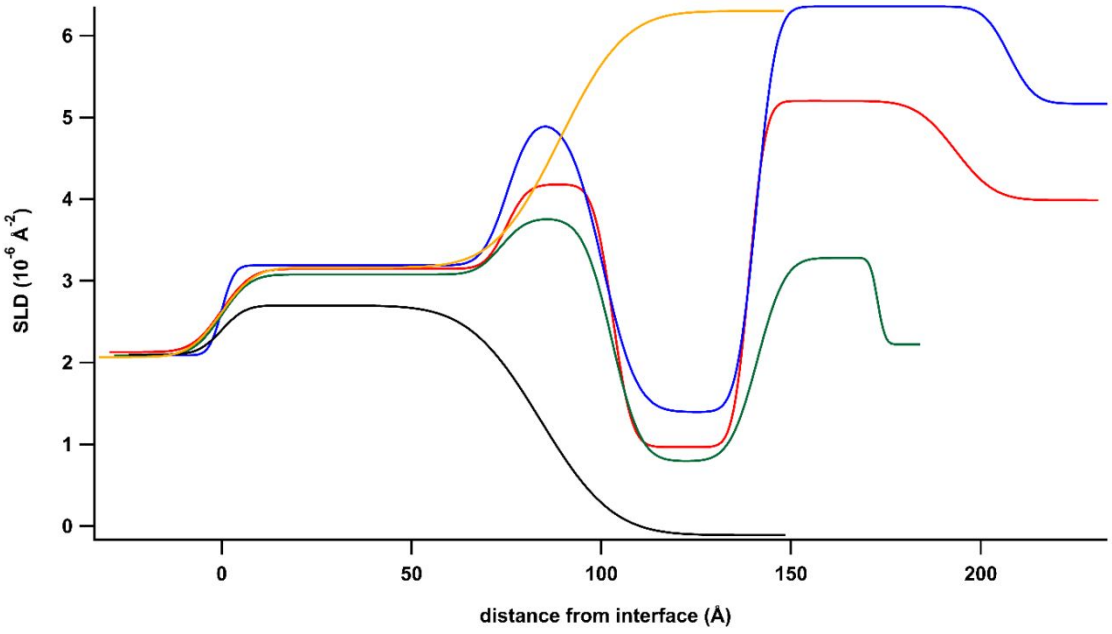


Figure 7 – Scattering length density profile of Dry (black), Wet (orange), 30% $D_2O$ (green), 60% $D_2O$ (red), and 80% $D_2O$ (blue) on hydrophilic Si Substrate.

Figures 7 and 8 show the scattering length density profiles of all three MEs near the

hydrophilic and amphiphilic surfaces, respectively. Figures 5 through 8 also show the reflectivity curves and scattering length density profiles resulting from the fitting process for each wafer dry (in the air) and in contact with $D_2O$. The structural details that derive from these fits for all samples studied on the hydrophilic and amphiphilic substrates are listed in Tables 2 and 3, respectively. All fits had a $\chi^2 < 10.5$. The scattering length density of each layer in the samples as determined by the reflectivity fits of the various compositions on a hydrophilic substrate are presented in Table 2, while the fits for compositions on the amphiphilic substrate are presented in Table 3. Moreover, the calculated SLDs of the components in the microemulsion or silicon wafer are presented in Table 4.

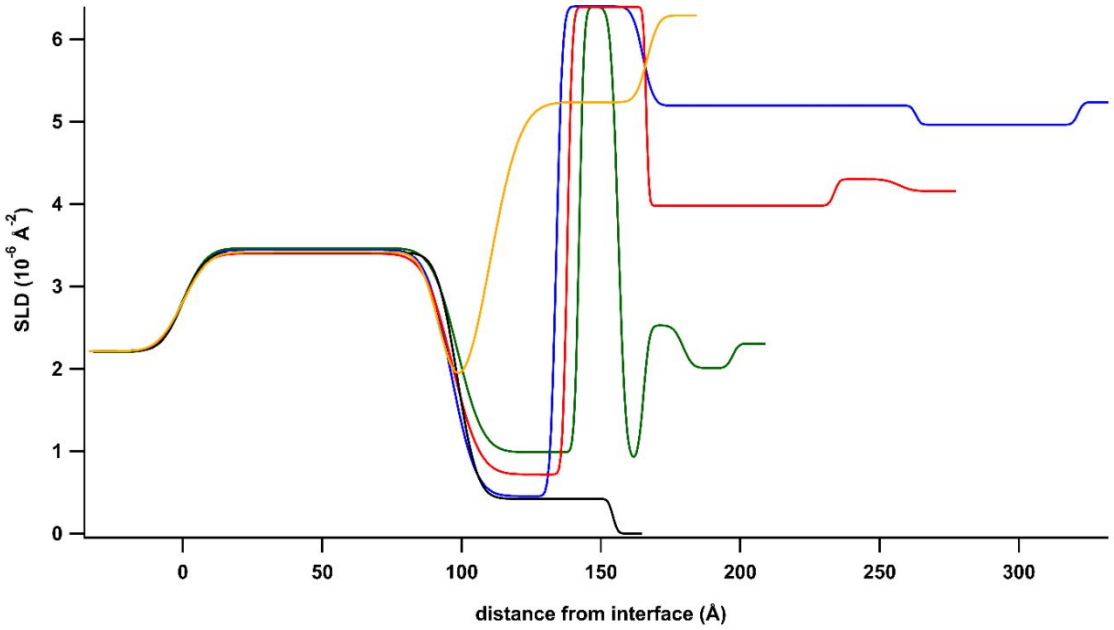


Figure 8 – Scattering length density profile of Dry (black), Wet (orange), 30% $D_2O$ (green), 60% $D_2O$ (red), and 80% $D_2O$ (blue) on amphiphilic Si Substrate.

*Impact of Si Substrate Hydrophilicity on Ordering*

Inspection of the results reveals the structure of the hydrophilic and amphiphilic silicon wafers in air and in $D_2O$. These results confirm an oxidized layer ($SiO_x$) on each substrate formed from treating the wafer with piranha and UV-Ozone. The hydrophilic substrate in the air has an oxidation layer that is 84 Å thick with an SLD of $2.700x10^{-6}$ Å$^{-2}$, which confirms the formation of $SiO_x$. For the Si substrate with the silane, the $SiO_x$ layer is 97 Å thick, with an SLD of $3.390x10^{-6}$ Å$^{-2}$.

The $SiO_x$ layer on the amphiphilic wafer transitions into a silane layer that is 51 Å thick with an SLD of $0.358x10^{-6}$Å$^{-2}$, which is higher than the estimated $SLD_{Silane} = -0.157x10^{-6}$ Å$^{-2}$. This variation can be attributed to the capture of moisture from the atmosphere attracted to the hydrophilic Si in both the silane and at the $SiO_x$ layer during this experiment. The thickness of the pure silane layer (51 Å) is also larger than the expected size of a dry n-octadecyltrimethoxysilane monolayer, which has been previously reported to be 21 Å and calculated from Avogadro Geometry Optimization to be 25 Å. Therefore, these results indicate that the silane forms multiple (2-3) layers on the Si surface during the silanization reaction.

When the hydrophilic surface is in contact with $D_2O$, the $SiO_x$ layer is hydrated, as evidenced by the SLD increasing to $3.164x10^{-6}$ Å$^{-2}$, while the layer thickness increased from 84 Å to 89 Å. This experiment also shows that a transition layer exists between the $SiO_x$ layer and the bulk $D_2O$, $SLD_{D_2O} = 6.393x10^{-6}$Å$^{-2}$. The SLD and thickness of the $SiO_x$ layer on the amphiphilic substrate did not vary with water. However, the silane layer did

Table 2 - Scattering length density (SLD x $10^{-6}$ Å$^{-2}$), thickness (z, Å), and roughness ($\sigma$, Å) of layers in microemulsions on hydrophilic Si substrate determined from reflectometry fits.

| Microemulsion | | SiOx | Layer 1 | Layer 2 | Layer 3 | Bulk |
|---|---|---|---|---|---|---|
| Dry $\chi^2$ <3.79 | SLD | 2.700 | - | - | - | 0.000 |
| | Z | 84.0 | - | - | - | - |
| | σ | 14.9 | - | - | - | 4.9 |
| Wet $\chi^2$ <3.31 | SLD | 3.164 | - | - | - | 6.302 |
| | Z | 89.1 | - | - | - | - |
| | σ | 6.8 | - | - | - | 13.5 |
| 80% $D_2O$ $\chi^2$ <4.36 | SLD | 3.190 | 4.537 | 1.230 | 6.360 | 5.169 |
| | Z | 75.2 | 31.7 | 39.2 | 70.4 | - |
| | σ | 2.6 | 5.7 | 2.1 | 4.3 | 5.6 |
| 60% $D_2O$ $\chi^2$ <4.03 | SLD | 3.149 | 4.036 | 0.967 | 5.202 | 3.988 |
| | Z | 75.0 | 31.2 | 36.1 | 54.3 | - |
| | σ | 6.1 | 4.3 | 4.0 | 3.4 | 8.1 |
| 30% $D_2O$ $\chi^2$ <3.45 | SLD | 3.079 | 3.767 | 0.793 | 3.283 | 2.223 |
| | Z | 73.6 | 29.2 | 38.4 | 31.7 | - |
| | σ | 5.9 | 5.2 | 6.0 | 5.8 | 1.6 |

contract when exposed to water, where the silane layer thickness decreases to 17 Å when exposed to water.

This collapse of the silane layer coupled with the emergence of an additional transitional layer between pure silane and pure $D_2O$ can be attributed to the adsorption of $D_2O$ into the top portion of the silane layer. Since the water contact angle is 66° on the silane, it is reasonable that water and oil may penetrate this layer to some extent.

Table 3 - Scattering length density (SLD x $10^{-6}$ Å$^{-2}$), thickness (z, Å), and roughness ($\sigma$, Å) of layers in microemulsions on amphiphilic silane substrate determined from reflectometry fits.

| Microemulsion | | SiOx | Layer 1 | Layer 2 | Layer 3 | Layer 4 | Layer 5 | Bulk |
|---|---|---|---|---|---|---|---|---|
| Dry $\chi^2$ <7.12 | SLD | 3.390 | 0.358 | - | - | - | - | 0.000 |
| | Z | 97.2 | 50.8 | - | - | - | - | - |
| | σ | 9.9 | 1.1 | - | - | - | - | 1.1 |
| Wet $\chi^2$ <10.17 | SLD | 3.416 | 1.249 | 5.236 | - | - | - | 6.289 |
| | Z | 92.6 | 17.3 | 56.7 | - | - | - | - |
| | σ | 7.2 | 5.6 | 8.8 | - | - | - | 3.2 |
| 80% $D_2O$ $\chi^2$ <3.53 | SLD | 3.445 | 0.453 | 6.399 | 5.194 | 4.963 | - | 5.236 |
| | Z | 96.2 | 37.8 | 31.1 | 98.0 | 58.1 | - | - |
| | σ | 6.8 | 7.1 | 1.7 | 3.0 | 1.4 | - | 1.5 |
| 60% $D_2O$ $\chi^2$ <4.05 | SLD | 3.398 | 0.717 | 6.392 | 3.981 | 4.301 | - | 4.156 |
| | Z | 96.6 | 41.4 | 28.3 | 67.5 | 23.2 | - | - |
| | σ | 6.7 | 7.9 | 1.4 | 0.8 | 1.5 | - | 3.9 |
| 30% $D_2O$ $\chi^2$ <3.72 | SLD | 3.464 | 0.987 | 6.390 | 0.880 | 2.527 | 2.009 | 2.305 |
| | Z | 98.5 | 43.7 | 14.0 | 9.1 | 14.1 | 17.7 | - |
| | σ | 6.7 | 7.3 | 1.3 | 2.1 | 1.6 | 2.7 | 1.7 |

While the oil will adsorb on the n-octadecyltrimethoxysilane chains, water is attracted to the Si attached to the substrate through the silane. Therefore, in a pure water environment, the silane may allow water to penetrate. The composition of this transitional layer appears to be dominated by $D_2O$, as its SLD is 5.236x$10^{-6}$ Å$^{-2}$. Moreover, the thickness of this transitional layer is 56.7 Å that, when combined with the thickness of the pure silane layer (17.3 Å), reveals that the silane layer partially swollen with water is *ca*. 23.2 Å thicker than the dry silane layer.

The final layers in the SLD profiles in Figures 7 and 8 are the bulk microemulsion and is not influenced by the presence of the surface. For dry substrates, this layer is air (SLD=0.000x$10^{-6}$ Å$^{-2}$), and for wet substrates, this layer is pure $D_2O$ (SLD=6.393x$10^{-6}$ Å$^{-2}$). For each ME, the composition and SLD of the final layers are dependent on the

Table 4 - Calculated scattering length density of components in microemulsion systems.

| Component | Density (g/cm$^2$) | SLD (x10$^{-6}$ Å$^{-2}$) |
|---|---|---|
| | | |
| Si | 2.329 | 2.073 |
| SiO | 2.130 | 2.897 |
| $SiO_2$ | 2.200 | 3.475 |
| $D_2O$ | 1.110 | 6.393 |
| Toluene | 0.867 | 0.941 |
| 1-butanol | 0.810 | -0.330 |
| polysorbate-20 | 1.100 | 0.594 |
| n-octadecyltrimethoxysilane | 0.883 | -0.155 |
| Emulsifier (82.5%vol. polysorbate-20/17.5%vol. 1-butanol) | *ca.* 1.049 | 0.432 |
| Protonated components of ME (10:1 ratio Emulsifier: Toluene) | *ca.* 1.031 | 0.483 |
| 30% $D_2O$/70% Protonated components of ME | *ca. 1.055* | 2.305 |
| 60% $D_2O$/40% Protonated components of ME | *ca.1.078* | 4.160 |
| 80% $D_2O$/20% Protonated components of ME | *ca. 1.094* | 5.236 |
| | | |

concentrations of water/surfactant/oil in the specific microemulsion. All of the layers between the surface and the bulk have lower SLDs than pure $D_2O$ and higher than that of the emulsifier/oil mix. In the following analysis and discussion, if the SLD of a layer is higher than that of the bulk microemulsion SLD, the layer is termed $D_2O$-rich. Conversely, if the layer has an SLD lower than the bulk solution, the layer is considered emulsifier-rich.

*Ordering of the Microemulsions on a Hydrophilic substrate*

The layered structure of all MEs on the hydrophilic surface, shown in Figure 7, exhibits similar trends, where each ME forms three layers between the silicon surface and the bulk microemulsion. Each ME produces a layer next to the $SiO_x$ layer with an SLD greater than

that of the $SiO_x$ layer. Such higher SLDs correspond to more $D_2O$, and the maximum SLD of each layer increases from $3.767x10^{-6}$ Å$^{-2}$, $4.036x10^{-6}$ Å$^{-2}$, and $4.537x10^{-6}$ Å$^{-2}$ as the $D_2O$ concentration increased from 30%, 60%, and 80%, respectively, in the microemulsion. The increased SLD in this layer indicates that the $D_2O$ is (unsurprisingly) attracted to the $SiO_x$ surface, although it is not pure $D_2O$ and therefore must be a mixture of $D_2O$ and oil/emulsifier. As the calculated SLDs of the components in the system are $6.393x10^{-6}$ Å$^{-2}$, $0.941x10^{-6}$ Å$^{-2}$, and $0.432x10^{-6}$ Å$^{-2}$ for $D_2O$, toluene, and the emulsifier, respectively, any layer with an SLD above $0.941x10^{-6}$ Å$^{-2}$ must contain some $D_2O$, and any layer with an SLD below $6.393x10^{-6}$ Å$^{-2}$ must contain some oil and/or surfactant. Therefore, the initial layer of the microemulsion on the hydrophilic surface appears to be a mixture of water and surfactant head groups. The SLD of this first layer scales with the amount of $D_2O$ in the system, further indicating that the amount of oil/surfactant in the layer neighboring the surface increases with a decrease in water concentration. Regardless of microemulsion composition, this initial layer is consistently around 30 Å thick, although increases in roughness when less water is in the system. This roughness may be attributed to the fact that at lower $D_2O$ concentrations, the lower contrast between layers results in a decrease in reflectivity, manifesting as an increase in interlayer roughness due to limited resolution between these layers.

The second layer that forms on the hydrophilic surface is mainly composed of emulsifier/oil, as indicated by the low SLD ($\sim 1 \times 10^{-6}$ Å$^{-2}$) of the layer. Only the 30% ME (SLD = $0.793x10^{-6}$ Å$^{-2}$) has a low SLD indicating the absence of water in this layer. Correspondingly, the 60% and 80% $D_2O$ samples each form a second layer with SLDs of $0.967x10^{-6}$ Å$^{-2}$ and $1.280x10^{-6}$ Å$^{-2}$, respectively, suggesting both layers have some $D_2O$ but

are predominately protonated oil/emulsifier. Similar to the layer next to the $SiO_x$, this layer retains an equal thickness for all $D_2O$ compositions (~37Å). At the same time, the roughness of the layering increases with the decrease in scattering intensity.

The third layer formed after the surfactant/oil-rich layer is another $D_2O$-rich layer, as indicated by the increase in SLDs above the bulk values of each microemulsion. This layer in the 80% $D_2O$ microemulsion is nearly pure $D_2O$, while the layers formed in the 30% and 60% microemulsions attain modest $D_2O$ concentrations. Additionally, the 80% $D_2O$ and 60% $D_2O$ have SLDs above the SLD of the layer adjacent to the $SiO_x$ surface and the bulk layer. In comparison, this layer in the 30% $D_2O$ microemulsion has an SLD lower than the layer near the $SiO_x$ but higher than the bulk microemulsion. Therefore, for the 30% $D_2O$ microemulsion, more water is present at the $SiO_x$-liquid interface than in the third layer.

Summarily, each ME forms three well-defined layers between the solid-liquid interface and the bulk solution on the hydrophilic surface. From the Si surface to the bulk, these layers alternate from a high concentration of $D_2O$ to an emulsifier/oil-rich layer followed by another water-rich layer. The compositions of these layers vary with ME composition as expected where more $D_2O$ is in the $D_2O$-rich layers for the MEs with higher water content. Additionally, the thicknesses of the first two layers do not vary with ME composition, while the thickness of the third layer scales with the amount of water in the ME.

*Microemulsion Ordering on an Amphiphilic Substrate*

The ordering of the MEs on the amphiphilic silane surface, as shown in Figure 8, organizes to a different structure than observed on the hydrophilic surface, Figure 7, while maintaining a similar general layering. On the silane surface, the analysis of the reflectivity

data shows the presence of the *ca.* 50 Å silane layer on the *ca.* 100 Å $SiO_x$ layer, as demonstrated in the SLD profiles of the dry (air) and wet ($D_2O$) samples. It is worth noting that the increase in the SLD of the silane layer in the presence of $D_2O$ indicates penetration of the $D_2O$ into the amphiphilic silane layer. When the 30%, 60%, and 80% $D_2O$ MEs are in contact with this amphiphilic surface, the contents of the ME, not just the $D_2O$, penetrate the silane, increasing its SLD to that of the emulsifier and oil as more ME penetrates the layer. Interestingly, the presence of the emulsifier and water appears to compress the silane layer. The 30% $D_2O$ ME compresses this layer to 44Å, while the 60% $D_2O$ (41Å) and 80% $D_2O$ (38Å) MEs compress the layer further. The SLD (and composition) of this layer also varies with ME composition, where the silane adsorbs the oil and emulsifier with less water in the microemulsion, raising the SLD of the layer above that of the pure silane. In all cases, the presence of the microemulsion compresses the thickness of the silane-surfactant/oil layer relative to that of the dry silane thickness.

A layer rich in $D_2O$ exists in all MEs that neighbors the silane-emulsifier/oil layer with SLDs between $6.389 \times 10^{-6}$ $Å^{-2}$ (30%) and $6.399 \times 10^{-6}$ $Å^{-2}$ (80%). This layer is present in all the MEs and has an SLD comparable to $D_2O$, indicative of a nearly pure $D_2O$ layer forming next to the silane-emulsifier/oil layer. However, the thickness varies with the concentration of $D_2O$. Careful inspection shows that this layer in the 80% $D_2O$ ME is at its thickest (31 Å), while decreasing slightly in the 60% $D_2O$ microemulsion to *ca.* 28 Å, and a thickness of 14 Å in the 30% $D_2O$ ME. Further from the silane layer beyond this $D_2O$-rich layer, each ME forms multiple layers with SLDs fluctuating between oil-rich and $D_2O$-rich before reaching the bulk ME. The number, depth, and breadth of the oscillations are directly correlated with the ME composition. The 80% $D_2O$ ME forms thick neighboring

layers of 98.0 Å and 58.1 Å, where the SLD of these layers ($5.194 \times 10^{-6}$ Å$^{-2}$ and $4.963 \times 10^{-6}$ Å$^{-2}$) are both slightly below the bulk microemulsion SLD of $5.236 \times 10^{-6}$ Å$^{-2}$. This suggests that in this ME, the compositions of these layers differ somewhat from that of the bulk and must form three-dimensional morphologies that connect the highly ordered layering at the surface to the tortuous bicontinuous morphology of the bulk. A decrease in water loading in the ME to 60% $D_2O$ leads to a similar structure, where two neighboring layers exist but are slightly thinner with layer thicknesses of 67.5 Å and 23.2 Å. Layers in the 60% $D_2O$ ME alternate from the SLD of the penultimate layer (SLD = $3.981 \times 10^{-6}$ Å$^{-2}$), being lower than the bulk (SLD = $4.16 \times 10^{-6}$ Å$^{-2}$), while the SLD of the last layer (SLD = $4.301 \times 10^{-6}$ Å$^{-2}$) increases back above that of the bulk. This alternating layering specifies that the concentration of each layer fluctuates between emulsifier-rich and $D_2O$-rich layers. Layers with SLDs closer to that of the bulk solution reveal the presence of both emulsifier/oil and $D_2O$ in these layers, suggesting the formation of three-dimensional morphologies that connect the highly ordered layering at the surface to the bulk bicontinuous morphology. The 30% $D_2O$ ME layers show a similar alternating structure, where the layers alternate in SLD below and above that of the bulk solution. However, in this ME, the layering decreases further in thickness (9.1 Å, 14.1 Å, and 17.7 Å), accompanied by an increase in the number of distinct layers from two to three. Furthermore, the change in SLD is more extreme ($8.80 \times 10^{-7}$ Å$^{-2}$, $2.527 \times 10^{-6}$ Å$^{-2}$, and $2.009 \times 10^{-6}$ Å$^{-2}$) before reaching the bulk solution (SLD = $2.305 \times 10^{-6}$ Å$^{-2}$). Interestingly, the total thickness of the three layers combined (41 Å) is similar to the estimated thickness of the domains of the surfactant channels measured by a collaborator in the bicontinuous bulk morphology (21 Å - 45 Å, which is the distance from one polysorbate-20 head group to the next polysorbate-20 head group). However, the

difference of SLDs between layers in the 30% $D_2O$ ME increases as compared to the 60% $D_2O$ and the 80% $D_2O$ ME, implying the layering is well defined between the emulsifier/oil-rich and $D_2O$-rich transitional layers, that is, the layers decrease in thickness but increase in richness of either emulsifier or $D_2O$.

## Comparison of experimental profile molecular simulations

To verify the fitting of the reflectivity data, we performed molecular dynamics simulations to compare the real space assembly of the microemulsion near hydrophilic and amphophilic surfaces to the fitted density profile. The computational results show a very similar ordering of the microemulsions near the surface, as well as provide real space pictures of the microemulsion assemblies.

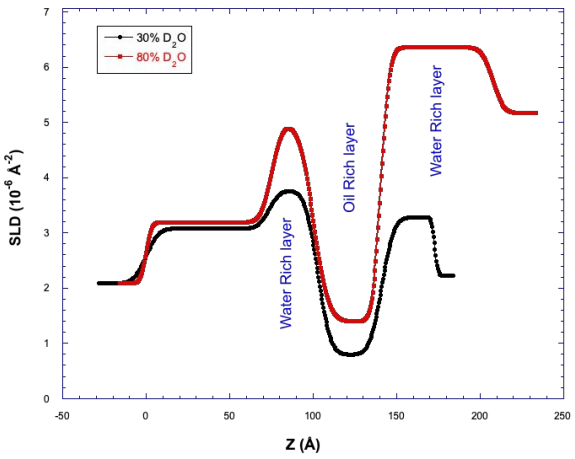


Fig 9 – scattering length density profile of the 30% and 80% $D_2O$ microemulsions on the hydrophilic surface

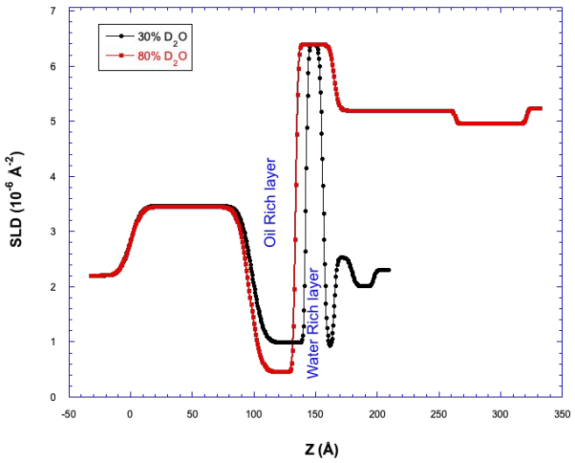


Fig 10 – scattering length density profile of the 30% and 80% $D_2O$ microemulsions on the amphiphilic surface

Figures 9 and 10 show the scattering length density profile of the reflectivity fits of the 30% and 80% $D_2O$ samples on the hydrophilic and amphiphilic surfaces, respectively, while Figures 11 and 13 present the density profile of the water and oil of these same samples from the computational studies on the amphiphilic and hydrophilic surfaces, respectively.

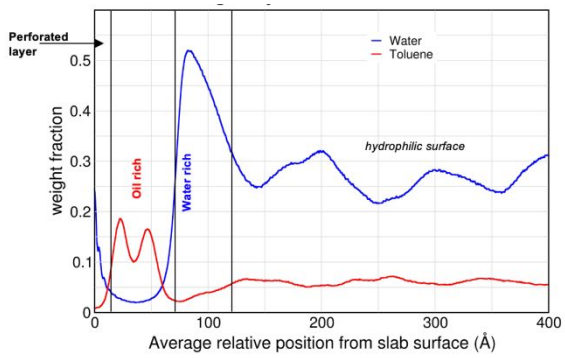


Fig 11 a – Density profile of the 30% $D_2O$ microemulsion on the hydrophilic surface from molecular dynamics simulation

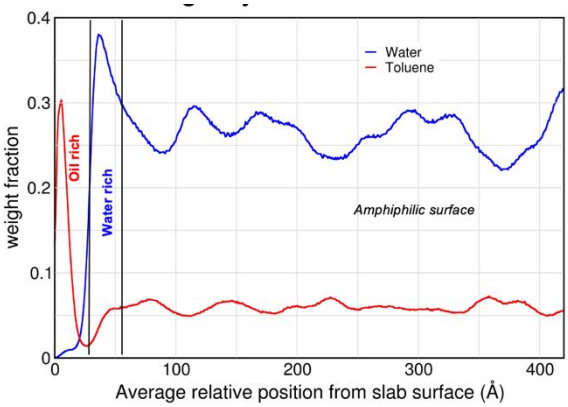


Fig 11 b – Density profile of the 30% $D_2O$ microemulsion on the amphiphilic surface from molecular dynamics simulation

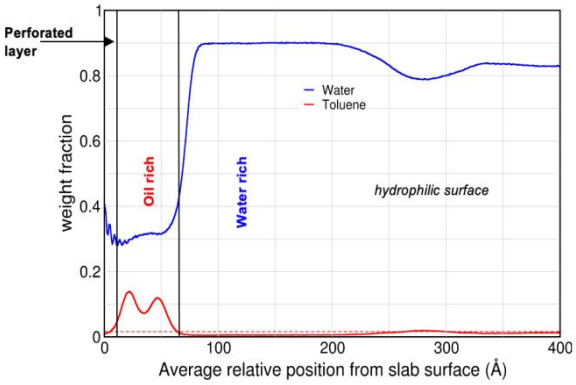


Fig 12 a – Density profile of the 80% $D_2O$ microemulsion on the hydrophilic surface from molecular dynamics simulation

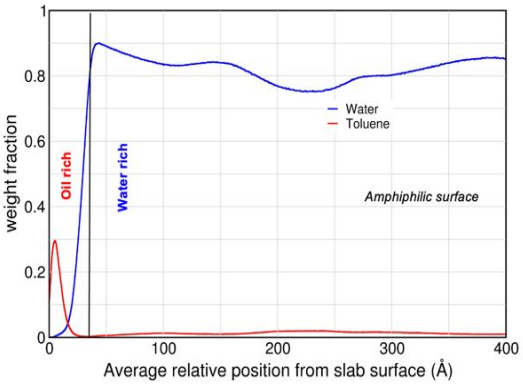


Fig 12 b – Density profile of the 80% $D_2O$ microemulsion on the amphiphilic surface from molecular dynamics simulation

Comparing Figures 9 and 11a shows strong similarity of layering of the oil and water in the 30% $D_2O$ on the hydrophilic surface. In both density profiles, there exists a narrow

layer (20-40 Å) that is water rich at the surface. This layer neighbors an oil rich layer (that is 40 Å- 50 Å), which is followed by a water rich layer that is also *ca.* 40-50 Å wide in both density profiles. In both the experimental and computational profiles, this near surface ordering then transitions into the bulk solution.

Similarly, comparison of Figure 9 with 12a shows that the computational and experimental density profiles of the 80% $D_2O$ microemulsion on the Hydrophilic surface are very similar. In both profiles, there exists a narrow layer (20-40 Å) that is water rich at the surface, where the concentration of water in this layer is more than that in the similar layer that exists near the hydrophilic surface for the 30% D2O microemulsion. In both the computational and experimental results, this layer neighbors a *ca.* 50 Å thick oil/polysorbate-20 rich layer which is followed a wider water rich layer that is ~ 60-100 Å wide. As in the ordering of the 30% $D_2O$ microemulsion near the hydrophilic surface, this near surface ordering then transitions into the bulk solutions.

Analogous inspection of the ordering of the 30% $D_2O$ microemulsion on amphiphilic surface as determined by reflectivity (Figure 10) or computationally (Figure 11b) shows that both techniques show a microemulsion that has an oil rich layer at the surface that is ~ 30-40 Å wide. In both studies, this near surface layer then neighbors a water rich layer of similar width that then transitions into an oscillating density profile towards the bulk composition. Finally, comparing the computational and experimental density profiles of the 80% $D_2O$ microemulsion on the amphiphilic surface show similar agreement. In both profiles (Figures 10 and 11b), there exists an oil rich layer at the surface that is ~ 30 Å wide, which neighbors a water rich layer that is richer in water than the 30 % $D_2O$

microemulsion sample. As with the previous samples, this near surface layering then transitions to the bulk composition with some modest oscillations of the density.

Thus, the computational studies validate the neutron reflectivity fits, showing analogous layering of the microemulsion near the surface to that found by the reflectivity experiments. More importantly, the computational studies provide a 3-dimensional picture of the distribution of the oil and water in this near surface ordering region, with a cross section shown in Figure 13 below, which renders the distribution of water and oil (left) and just water (right) in the 30% $D_2O$ microemulsion near the hydrophilic surface. This picture illustrates how the components of the microemulsion preferentially arrange near the surface, exemplifying that all layers are a mixture of water and oil. Moreover, the distribution of the water shows a clear perforated lamellae type structure of the bicontinuous assembly near the surface. It is worth noting that additional information regarding the lateral ordering of the microemulsion can be garnered from grazing incidence x-ray or neutron scattering studies and this may be an interested follow-on study,

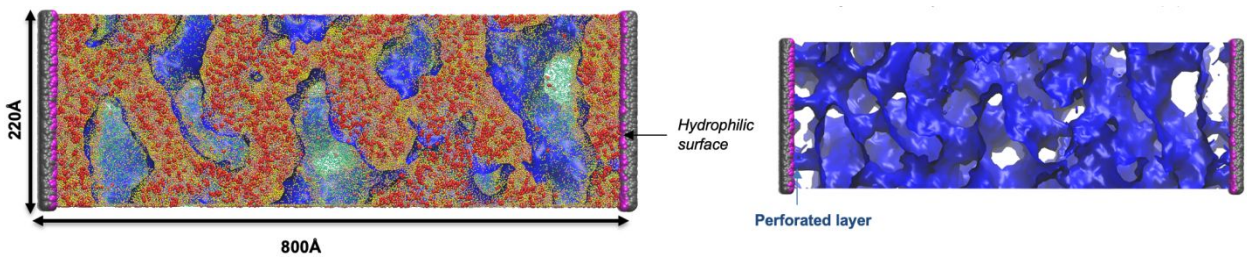


Figure 13 – 3-Dimensional structure of the 30% $D_2O$ microemulsion near the hydrophilic surface exemplifying the perforated structure near the surface.

## Discussion

### *Hydrophilic surface structures*

The neutron reflectivity and simulation results clearly show that each ME forms three definite layers on the hydrophilic surface before reaching the bulk composition at 175-200 Å from the silicon wafer surface. The layer closest to the $SiO_x$ surface is a mixture of emulsifiers and $D_2O$, and the amount of $D_2O$ in this layer increases with increasing $D_2O$ loading in the ME. However, this initial layer is not $D_2O$-rich for the 60% and 80% $D_2O$ MEs, as the peak SLD for this layer is less than the bulk ME. Unfortunately, the composition of the layer does not precisely identify the morphology of the ME at the surface. However,

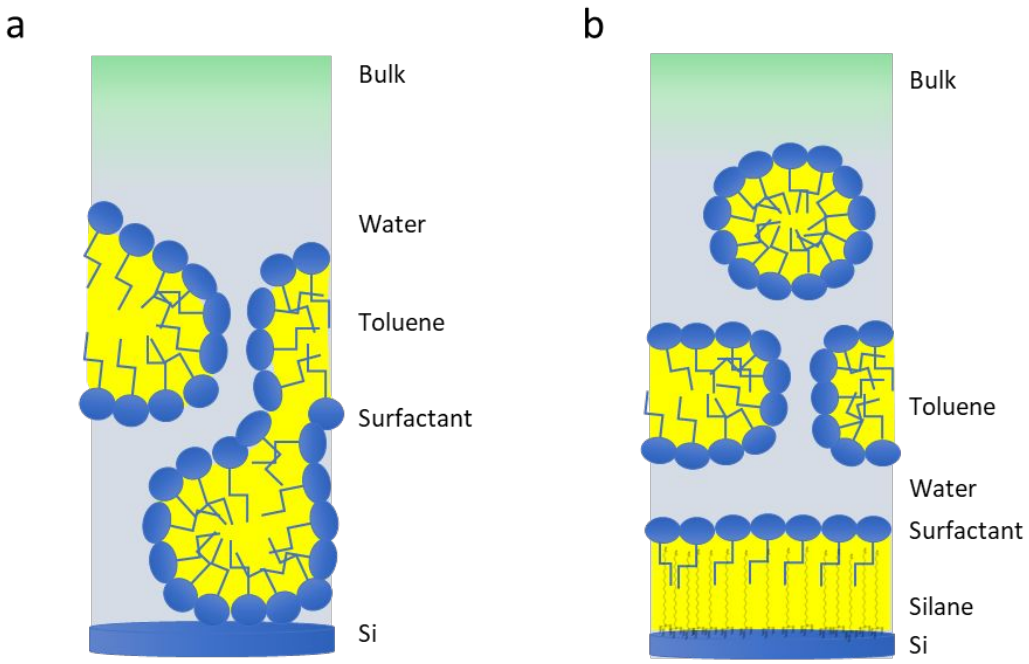


Figure 14 – Sketch of proposed microemulsion structures at a hydrophilic Si surface (a) and amphiphilic silane surface (b), illustrating how lamellar may form with perforations as they approach the bulk solution.

careful interpretation of the layers can provide insight into the ME structure in the near-surface layers.

$D_2O$ and the hydrophilic headgroups of the surfactant are attracted to the hydrophilic $SiO_x$ surface, creating a mixed layer that contains water and surfactant. One morphology, illustrated in Figure 14 a, consistent with this mixed layer, contains elongated droplet-like surfactant aggregates enclosing oil in a continuous water phase. This assembly has been suggested in previous studies of microemulsions and creates perforations in the water lamellae by oil/surfactant droplets.[Error! Reference source not found.,Error! Reference source not found.] These perforations can be considered channels between layers of oil and water separated by surfactant boundaries, forming the BME channels. As the concentration of water decreases, the volume fraction of the surfactant head groups on this layer increases, consistent with the decreasing SLD of this layer as the ME composition changes from 80% to 60% and 30% $D_2O$. Moreover, the thickness of this layer remains around 31 Å, which is near the reported size of the surfactant molecule, 35 Å,[4,7], suggesting the size of the surfactant molecule and its alignment (nearly) perpendicular to the surface controls the thickness of this layer.

The transition from the first to the second layer consists of a mixture of hydrated surfactant headgroups and oil with the surfactant tails, then transitioning to an oil-rich layer. However, this second layer consists primarily of oil and surfactant. At higher $D_2O$ concentrations, the SLD increases, which can be attributed to small water channels throughout the continuous surfactant/oil layer. The SLD of this layer in the 30% $D_2O$ ME indicates the layer is dominated by emulsifier and toluene. The SLD of this layer in the 60% and 80%$D_2O$ ME is higher, corresponding to increased $D_2O$ in this layer. The increased

amount of $D_2O$ appears to drive the surfactant to enclose a region of toluene in the layer, allowing small pockets of $D_2O$ to exist in this layer. Our interpretation is that these pockets of $D_2O$ are the beginning of perforations that form as the distance from the solid-liquid interface increases.

The initial layers formed are distinct and may have droplets of oil/emulsifiers in water or hydrated surfactant heads. However, further from the surface, the SLD of the layers approach that of the bulk through dampening fluctuations in SLD. A Layer with an SLD closer to the bulk SLD indicates a layer that has a composition that more closely resembles the bulk solution. Therefore, we envision that as the SLD approaches the bulk, perforations of oil in $D_2O$-rich layers or $D_2O$ in oil-rich layers increase gradually, transitioning to the bulk solution where oil and water channels with the emulsifier at the interface have formed the bicontinuous morphology.

The third layer that forms in the MEs on a hydrophilic surface has SLDs that indicate a $D_2O$-rich layer, where the amount of $D_2O$ in the layer increases with ME $D_2O$ content. In the 80% $D_2O$ ME, the layer is almost pure $D_2O$ and thicker than any other layer discussed yet. The dominant presence of water in this layer forms a lamella structure encompassed by the surfactant/oil-rich layer closer to the surface and the bulk microemulsion further from the surface. Inspection of this layer in the 60% $D_2O$ ME shows a thinner layer and a lower SLD than the 80% $D_2O$ ME. Hence, this layer is a mixture of emulsifier/oil and $D_2O$, which suggests that it contains emulsifier/oil aggregates in a primarily $D_2O$ layer, forming perforations of the water layer. The structure of this layer in the 30% $D_2O$ ME further

suggests that perforations of emulsifier/oil aggregates are developing in the $D_2O$-rich lamellae. In this layer, the SLD is still above that of the bulk SLD and is mostly water.

Overall, the MEs form a triple layer assembly on the hydrophilic surface, alternating between $D_2O$-rich, emulsifier/oil-rich, and $D_2O$-rich layers. In the $D_2O$-rich layers, increased $D_2O$ loading in the ME corresponds to higher $D_2O$ loading in each layer. The layers are not pure $D_2O$ or emulsifier/oil, indicating that droplets of the minor phase perforate the layers. Additionally, the transitions between surfactant-rich and $D_2O$-rich layers are gradual, consistent with channels between the layers.

*Ordering of the Microemulsions on the Amphiphilic surfaces*

On the amphiphilic surface, the MEs assemble slightly differently than on the hydrophilic surface. The amphiphilic surface contains a grafted silane layer that forms the first layer near the $SiO_x$ layer. This silane layer is penetrated by the emulsifier and oil while compressed by the $D_2O$, resulting in a decrease in SLD and layer thickness with increasing $D_2O$. Adsorption of oil and emulsifier in the silane at this layer suggests that primarily the hydrophobic surfactant tails and oil of the ME forms penetrate the silane with minimal $D_2O$ entering. We interpret the sharp transition from the silane to the neighboring ME layer to suggests that polysorbate-20 surfactant heads align to form a nearly parallel boundary, with the surfactant tails aligning perpendicularly to the surface and the surfactant bordering the adjacent $D_2O$-rich layer. In all three MEs, the $D_2O$-rich layer is well-defined and nearly pure, which indicates the layering of the MEs on the amphiphilic surface is more definitive than their ordering of the hydrophilic surface.

These initial layers near the hard surface transition to multiple (2-3) layers that oscillate in composition (and SLD) above and below that of the bulk microemulsion. These layers in the 80% and 60% $D_2O$ microemulsion contain $D_2O$-rich lamellae intermixed with patches of emulsifier/oil, or vice-versa. An additional layer is present in the 30% $D_2O$ microemulsion, where each layer decreases in thickness that dampen as they approach the bulk. These features suggest that the microemulsions form elongated surfactant aggregates in these layers at higher water content. These aggregates act as the boundaries between oil and water channels and increase volume fraction as the layers approach the bulk solution, as illustrated in Figure 14b. Interestingly, the SLD only varies slightly from the SLD of the bulk ($\pm$ 5%) in these layers, indicating that the layering in this area is not determinate for the 60% and 80% MEs. However, in the 30% $D_2O$ microemulsion, the SLD oscillations beyond the first two layers are more significant (+10%, -50%), indicating that more defined layers form in these MEs and perforations in these layers are fewer than at higher $D_2O$ loadings.

*Impact of Surface Structures on Electrochemical Performance*

For electrolysis to occur in a conductive solution at a sufficient applied potential, the redox species must approach the electrode surface within a suitable distance for electron transfer, and local electroneutrality must be maintained. In microemulsions with aqueous supporting electrolyte and oil-solubilized redox species, the solution structure near the electrode determines whether these criteria are met. Therefore, static measurements of the near-surface structures of microemulsions provide insight into the applicability of microemulsions as electrolytes. The presence of mixed layers on a surface should provide

pathways for diffusion of nonpolar redox species to reach the electrode and transport of ions to maintain electroneutrality. In addition, several processes will typically accompany electron transfer at the electrode surface. The coupling of ion transport and electrochemical reaction steps may entail mechanisms such as proton transfer to electrolytically-generated anions, transfer of supporting electrolyte ions from the aqueous to the oil phase, transfer of redox molecule from oil to aqueous phase following electron transfer, or migration of charged redox species towards charged headgroups of surfactant.

Due to the electrowetting phenomenon, it is probable that even amphiphilic electrodes, such as glassy carbon, gold, and platinum, would behave similarly to a hydrophilic electrode under a potential bias.[44,45] Therefore, the hydrophilic surface-microemulsion model is expected to better describe the microemulsion layering on glassy carbon, platinum, and gold electrodes used in electrochemical experiments. On the hydrophilic surface, 30%, 60%, and 80% $D_2O$ MEs assemble into mixed layers near the surface that are consistent with perforated lamellae. The presence of coexisting aqueous and oil domains near a surface provides independent paths for ion and redox species transport and enables electrochemical reactions. While electroneutrality must be satisfied for electron transfer reactions to occur, there are two possible mechanisms: (1) transfer of electrolytically generated species from the oil phase to the aqueous phase or (2) transfer of ions into the oil phase. It has previously been shown that decamethylferrocene cations, generated electrochemically in toluene emulsion droplets, readily transfer from the toluene to the aqueous phase, following the latter mechanism.[25] The facility with which an ion generated in the oil phase is transferred to the aqueous phase is quantified by the driving force

needed for the electrochemical reaction, the redox potential ($E^0 \approx E_{1/2}$). Using ferrocene as an electrochemical probe in this microemulsion system, we demonstrate a cathodic shift in the $E_{1/2}$ with increasing microemulsion water content on glassy carbon, platinum, and gold electrodes (Figure 15). As shown above on the hydrophilic surface, as the water content in microemulsions increases from 30% to 80%, the layer adjacent to the surface becomes increasingly water rich, as demonstrated in the reflectivity analysis. The increase in local water content facilitates increased transfer of ferrocenium from the oil to the aqueous phase, which reduces the magnitude of the applied potential needed to drive the reaction, a classic 'following reaction' effect.[4,17] Thus, increased availability and mixing of emulsifier/oil and water at the surface in perforated lamellae should increase the charge transfer in the structures of these systems.

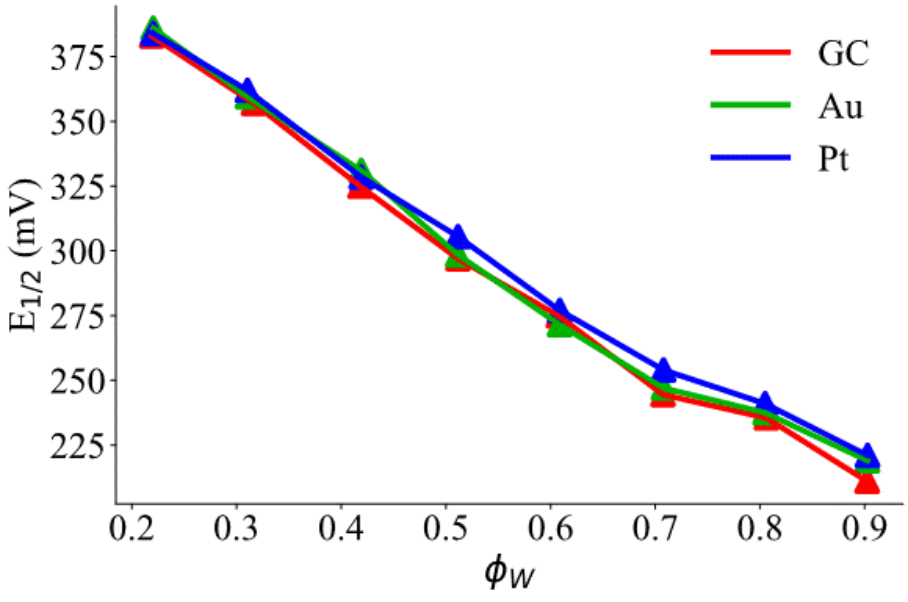


Figure 15 - $E_{1/2}$ as a function of microemulsion water fraction determined from cyclic voltammetry using a 10mV/s scan rate and a glassy carbon, gold, or platinum

Finally, it must be noted that these measurements monitor the structure of a static sample with no external electric field. The application of an electric field and the inclusion of ferrocene is expected to alter these assemblies and alter charge transfer performance to follow the $E_{1/2}$ trends. Future experiments are planned to examine the assembly of microemulsions near various surfaces in an electric field.

## Conclusions

The assembly of bicontinuous microemulsions near surfaces with varying hydrophilicity is monitored in this study. Structures of different compositions of bicontinuous microemulsions on hydrophilic and amphiphilic substrates have been determined. The microemulsions (MEs) examined here form multiple lamellar-like layers on hydrophilic and amphiphilic surfaces, where each layer is rich in water or emulsifier/oil. The layers transition to bulk material over 100-200 Å, where the layers can be described as perforated lamellae. MEs on the hydrophilic surface form layers consistent with perforated lamellae for all compositions studied. On the hydrophilic surface, increased $D_2O$ content forms thick $D_2O$-rich layers that may inhibit charge transfer. However, on the amphiphilic surface, the microemulsions form more layers that are mixed in water or oil/emulsifier. Therefore, the MEs on the hydrophilic surface create perforated lamellar assemblies that provide pathways that should improve charge transfer near the surface.

The thicknesses of the layers decrease with decreased water content in these MEs on both surfaces. The 30% $D_2O$ ME forms thinner layers relative to those formed in the 60% $D_2O$ and 80% $D_2O$ microemulsions, primarily when in contact with an amphiphilic surface. Finally, the observed multiple mixed layers between the surfaces and the bulk solution are

accordant with the existence of perforated lamellae, which is consistent with the presence of multiple pathways to maintain conductivity and electroneutrality during electron transfer with a nonpolar probe.

## Acknowledgments

This work was supported as part of the Breakthrough Electrolytes for Energy Storage (BEES), an Energy Frontier Research Center funded by the U.S. Department of Energy, Office of Science, Basic Energy Sciences under Award# DE-SC0019409. We acknowledge the support of the National Institute of Standards and Technology, U.S. Department of Commerce, in providing the neutron research facilities used in this work.

## References


1 Kalaitzaki A, Emo M, Stebe MJ, Xenakis A, Papadimitriou V. Biocompatible nanodispersions as delivery systems of food additives: A structural study. Food Research International. 2013;54(2):1448-1454.

2 del Rio JG, Hayes DG, Urban VS. Partitioning behavior of an acid-cleavable, 1,3-dioxolane alkyl ethoxylate surfactant in single and binary surfactant mixtures for 2-and 3-phase microemulsion systems according to ethoxylate head group size. Journal of Colloid and Interface Science. 2010;352(2):424-435

3 Lawrence MJ, Rees GD. Microemulsion-based media as novel drug delivery systems. Advanced Drug Delivery Reviews. 2000;45(1):89-121.

4 Peng J, Cantillo NM, Nelms KM, Roberts LS, Goenaga G, Imel A, Barth BA, Dadmun M, Heroux L, Hayes DG, Zawodzinski T Electron Transfer in Microemulsion-Based Electrolytes. ACS Applied Materials & Interfaces. 2020;12(36):40213-40219

5 Kunitake M, Kuraya E, Kato D, Niwa O, Nishimi T. Electrochemistry in bicontinuous microemulsions based on control of dynamic solution structures on electrode surfaces. Current Opinion in Colloid & Interface Science. 2016;25:13-26

6 Moumen N, Pileni MP, Mackay RA. Polymerization of methacrylate in a W O microemulsion stabilized by a methacrylate surfactant. Colloids and Surfaces a-Physicochemical and Engineering Aspects. 1999;151(3):409-417.

7 Mackay RA, Myers SA, Bodalbhai L, Brajtertoth A. Microemulsion structure and its effect on electrochemical reactions. Analytical Chemistry. 1990;62(10):1084-1090.

8 Kulkarni V, Shaw C. Essential Chemistry for Formulators of Semisolid and Liquid Dosages, Chapter 2 - Surfactants, Lipids, and Surface Chemistry, Page: 5-19 2016

9 Torrealba VA, Hoteit H, Johns RT. Description of Micellar Radii for Phase Behavior and Viscosity Modeling of Aqueous Surfactant Solutions and Microemulsions. Langmuir. 2018;34(50):15327-15334.

10 Makita Y, Uemura S, Miyanari N, Kotegawa T, Kawano S, Nishimi T, Tominaga M, Nishiyama K, Kunitake M Electrochemical Investigation of Dynamic Solution Structures of Bicontinuous Microemulsion at Solid Interfaces. Chemistry Letters. 2010;39(11):1152-1154.

11 Vargas-Ruiz S, Soltwedel O, Micciulla S, Sreij R, Feoktystov A, von Klitzing R, Hellweg T, Wellert S Sugar Surfactant Based Microemulsions at Solid Surfaces: Influence of the Oil Type and Surface Polarity. Langmuir. 2016;32(45):11928-11938.

12 Torikai N, Yamada NL, Noro A, Harada M, Kawaguchi D, Takano A, Matsushita Y Neutron reflectometry on interfacial structures of the thin films of polymer and lipid. Polymer Journal. 2007;39(12):1238-1246

13 Kuraya E, Nagatomo S, Sakata K, Kato D, Niwa O, Nishimi T, Kunitake M Simultaneous Electrochemical Analysis of Hydrophilic and Lipophilic Antioxidants in Bicontinuous Microemulsion. Analytical Chemistry. 2015;87(3):1489-1493

14 Lipfert F, Kerscher M, Mattauch S, Frielinghaus H. Stability of near-surface ordering of bicontinuous microemulsions in external shear-fields. Journal of Colloid and Interface Science. 2019;534:31-36.

15 Kawano S, Kobayashi D, Taguchi S, Kunitake M, Nishimi T. Construction of Continuous Porous Organogels, Hydrogels, and Bicontinuous Organo/Hydro Hybrid Gels from Bicontinuous Microemulsions. Macromolecules. 2010;43(1):473-479

16 Mackay RA, Dixit NS, Hermansky C, Kertes AS. Conductivity and diffusion measurements in micellar and o/w microemulsion systems - a comparative-study. Colloids and Surfaces. 1986;21:27-39.

17 Imel A, Barth B, Hayes D, Dadmun M, Zawodzinski T. Microemulsions as Emerging Electrolytes: The Correlation of Structure to Electrochemical Response ACS Appl. Mater. Interfaces 2022, 14, 17, 20179–20189.

18 Xie S, Meyer D, Wang E, Bates F, Lodge T, Structure and Properties of Bicontinuous Microemulsions from Salt-Doped Ternary Polymer Blends, Macromolecules 2019, 52, 9693-9702.

19 Schneider K, Verkoyen P, Krappel M, Gardiner C, Schweins R, Frey H, Sottman T, Efficiency Boosting of Surfactants with Poly(ethylene oxide)-Poly(alkyl glycidyl ether)s: A New Class of Amphiphilic Polymers, Langmuir 2020, 36, 9849-9866.

20 Huo L, Du P, Zhou H, Zhang K, Liu P. Fabrication and tribological properties of self-assembled monolayer of n-alkyltrimethoxysilane on silicon: Effect of SAM alkyl chain length. Applied Surface Science 396 (2017) 865–869

21 Zhou XL, Chen SH. Theoretical foundation of x-ray and neutron reflectometry. Physics Reports-Review Section of Physics Letters. 1995;257(4-5):223-348

22 Engstrom R, Strasser V, Characterization of Electrochemically Pretreated Glassy Carbon Electrodes, Anal. Chem, 1984; 56: 136-141

23 Zhou XL, Lee LT, Chen SH, Strey R. Observation of surface-induced layering in bicontinuous microemulsions. Physical Review A. 1992;46(10):6479-6489

24 Kerscher, M,Busch, P, Mattauch, S, Frielinghaus, H, Richter, D, Belushkin, M, Gompper, G. Near-surface structure of a bicontinuous microemulsion with a transition region. Phys. Rev. E . 2011;83(3):030401

25 Deng HQ, Dick JE, Kummer S, Kragl U, Strauss SH, Bard AJ. Probing Ion Transfer across Liquid-Liquid Interfaces by Monitoring Collisions of Single Femtoliter Oil Droplets on Ultramicroelectrodes. Analytical Chemistry. 2016;88(15):7754-7761.

26 Nevot L, Croce P. Characterization of surfaces by grazing x-ray reflection - application to study of polishing of some silicate-glasses. Revue De Physique Appliquee. 1980;15(3):761-779

27 Parratt LG. Surface studies of solids by total reflection of x-rays. Physical Review. 1954;95(2):359-369.

28 Maranville B, Ratcliff II W, Kienzle P Reductus: a stateless Python data reduction service with a browser front end. Journal of Applied Crystallography (2018);51: 1500-1506

29 Nelson A. Co-refinement of multiple-contrast neutron/X-ray reflectivity data using MOTOFIT. Journal of Applied Crystallography. 2006;39:273-276.

30 Souza, P.C., et al., *Martini 3: a general purpose force field for coarse-grained molecular dynamics.* Nature methods, 2021. **18**(4): p. 382-388.

31 Grunewald, F., et al., *Transferable MARTINI model of poly (ethylene oxide).* The journal of physical chemistry B, 2018. **122**(29): p. 7436-7449.

32 Katiyar, P. and J.K. Singh, *A coarse-grain molecular dynamics study of oil–water interfaces in the presence of silica nanoparticles and nonionic surfactants.* The Journal of Chemical Physics, 2017. **146**(20).

33 Tang, X., K.J. Huston, and R.G. Larson, *Molecular dynamics simulations of structure–property relationships of Tween 80 surfactants in water and at interfaces.* The Journal of Physical Chemistry B, 2014. **118**(45): p. 12907-12918.

34 Brandner, J.D., *The composition of NF-defined emulsifiers: Sorbitan monolaurate, monopalmitate, monostearate, monooleate, polysorbate 20, polysorbate 40, polysorbate 60, and polysorbate 80.* Drug development and industrial pharmacy, 1998. **24**(11): p. 1049-1054

35 Borisov, O.V., et al., *Toward understanding molecular heterogeneity of polysorbates by application of liquid chromatography–mass spectrometry with computer-aided data analysis.* Analytical chemistry, 2011. **83**(10): p. 3934-3942.

36 Amani, A., et al., *Molecular dynamics simulation of a polysorbate 80 micelle in water.* Soft Matter, 2011. **7**(6): p. 2900-2908.

37 Rossi, G., et al., *A coarse-grained MARTINI model of polyethylene glycol and of polyoxyethylene alkyl ether surfactants.* The Journal of Physical Chemistry B, 2012. **116**(49): p. 14353-14362.

38 Pérez-Sánchez, G., et al., *Coarse-grain molecular dynamics simulation framework to unravel the interactions of surfactants on silica surfaces for oil recovery.* Colloids and Surfaces A: Physicochemical and Engineering Aspects, 2023. **670**: p. 131583.

39 Pandey, Y.N. and M. Doxastakis, *Detailed atomistic Monte Carlo simulations of a polymer melt on a solid surface and around a nanoparticle.* The Journal of chemical physics, 2012. **136**(9).

40 Van Der Spoel, D., et al., *GROMACS: fast, flexible, and free.* Journal of computational chemistry, 2005. **26**(16): p. 1701-1718.

41 Bernetti, M. and G. Bussi, *Pressure control using stochastic cell rescaling.* The Journal of Chemical Physics, 2020. **153**(11)

42 Humphrey, W., A. Dalke, and K. Schulten, *VMD: visual molecular dynamics.* Journal of molecular graphics, 1996. **14**(1): p. 33-38.

43 Lopian, T., et al., *Morphologies Observed in Ultraflexible Microemulsions with and without the Presence of a Strong Acid.* ACS central science, 2016. **2**(7): p. 467-475.

44 Calfumán K, Honores J, Isaacs M, Quezada D, Valdebenito J, Urzúa M Quick and Easy Modification of Glassy Carbon Electrodes with Ionic Liquid and Tetraruthenated Porphyrins for the Electrochemical Determination of Atrazine in Water. Electroanalysis 2019;31:671-677

45 Hayes, R., Feenstra, B. Video-speed electronic paper based on electrowetting. Nature 2003;425 :383–385

Data Availability Statement

- The data supporting this article have been included as part of the Supplementary Information.